Flow of Non-Newtonian Polymeric Solutions Through Fibrous Media

B.N. DHOTKAR,[1] R. P. CHHABRA[1], V. ESWARAN[2]

[1]Department of Chemical Engineering, Indian Institute of Technology, Kanpur, India 208016

[2]Department of Mechanical Engineering, Indian Institute of Technology, Kanpur, India 208016

Received 19 April 1999; accepted 16 September 1999

ABSTRACT: The equations of motion (continuity and momentum) describing the steady flow of incompressible power law liquids in a model porous medium consisting of an assemblage of long cylinders have been solved numerically using the finite difference method. The field equations as well as the pertinent boundary conditions have been re-cast in terms of the stream function and vorticity. The inter-cylinder interactions have been simulated using a simple "concentric cylinders" cell model. Extensive information on the detailed structure of the flow field in terms of the surface vorticity distribution, streamlines, and viscosity distribution on the surface of the solid cylinder as well as on the values of the pressure and friction drag coefficients under wide ranges of physical ($0.4 \leq \epsilon \leq 0.95$; $1 \geq n \geq 0.4$) and kinematic ($0.01 \leq Re \leq 10$) conditions have been obtained. The numerical results presented herein have been validated using the experimental results for the flow of Newtonian and power law fluids available in the literature; the match between the present predictions and the experiments was found to be satisfactory. © 2000 John Wiley & Sons, Inc. J Appl Polym Sci 76: 1171–1185, 2000

Key words: fibrous beds; power law fluids; pressure drop; drag; bundle of cylinders

INTRODUCTION

The steady flow of incompressible non-Newtonian polymeric systems (melts and solutions) relative to an array of long cylinders represents an idealization of many industrially important processes frequently encountered in polymer and chemical engineering applications. For instance, in the commonly used autoclave process of manufacturing fiber reinforced composites, the flow of resin through a bed of fibers accompanied by consolidation denotes an important step in the overall process.[1–3] Other examples where this flow configuration is encountered include paper and textile coating operations, the filtration of polymer melts using a bed of screens prior to various shaping and molding operations,[4] enhanced oil recovery via polymer flooding,[5] the flow in the shell of tubular heat exchangers and the membrane modules,[6–8] and so on. Finally, the flow through an array of cylinders has also been frequently used to mimic the flow of non-Newtonian fluids in porous medium to elucidate the role of the successive convergent-divergent nature of the flow passages.[9–12] Owing to its overwhelming pragmatic and theoretical significance, over the years considerable research effort has been directed at developing a better understanding of the flow of fluids through such a model system, which in turn facilitates the understanding of flow in real fibrous porous media. Consequently, a wealth of information is now available relating to the flow of Newtonian fluids, which has been reviewed by several authors.[1,13] Clearly, the estimation of the fluid

Correspondence to: R. P. Chhabra.

Journal of Applied Polymer Science, Vol. 76, 1171–1185 (2000)

dynamic resistance to the flow of a fluid represents one of the most important design parameters. This information is conveniently expressed in terms of either a permeability of the system or a drag coefficient or in terms of a friction factor. Obviously all of these are inter-related and are not mutually exclusive, at least in the low Reynolds number region. Based on the detailed comparisons presented in the literature, it is perhaps fair to state that satisfactory methods of estimating the resistance to flow of Newtonian fluids in such model fibrous media are now available in the literature (e.g., see refs. 13,14). In contrast to this, much less is known about the analogous flow of non-Newtonian fluids in this flow geometry, and the present study represents a step in the direction of bridging this gap in the existing literature. However, before undertaking a detailed discussion of this study, it is useful and instructive to briefly summarize the salient features of the previous studies available in this field.

PREVIOUS WORK

In spite of the aforementioned overwhelming importance of this flow configuration in relation to many applications in polymer processing, the flow of non-Newtonian fluids relative to an array of long cylinders has received only very limited attention, both analytically as well as experimentally, whereas the pertinent literature for Newtonian fluids has been reviewed recently.[13,14] As far as known to us, there have been only three theoretical analyses reported in the literature. Skartsis et al.[15] have numerically studied the flow of power law fluids normal to square arrays of different spacing (characterized in terms of an overall mean value of voidage) composed of long cylinders and they reported fair agreement with the predicted and experimental values of the resistance to flow expressed in terms of a dimensionless Kozeny coefficient, for the limited range of conditions of porosity and power law index studied. On the other hand, Tripathi and Chhabra[14,16] employed the well known variational principles and obtained upper and lower bounds on the flow resistance as a function of the bed porosity and rheological parameters for both power law and Carreau viscosity models under wide range of conditions. In the latter studies, a cell model was used to simulate the inter-cylinder interactions. Detailed comparisons between these predictions and experimental results for the flow of Newtonian fluids through fibrous media demonstrate the general applicability of this approach.[14,16,17] However, the corresponding comparisons for power law fluids were seen to be not only very limited but also less satisfactory. One possible reason is the approximate nature of the upper and lower bounds themselves that increasingly diverge as the degree of shear thinning behavior of the fluid increases, albeit the possible viscoelastic effects present in the some of scant experimental results cannot be ruled out. In addition, there is really no justification for using the arithmetic mean of the upper and lower bounds. All these studies relate to the so-called creeping flow only, i.e., zero Reynolds number and hence are applicable only at low Reynolds number of flow. On the other hand, Adams and Bell[6] and Prakash et al.[7] have reported the experimental values of the resistance to flow of purely viscous polymer solutions for in-line and staggered square arrays of cylinders, and both of them put forward empirical expressions for friction factor encompassing moderate values of Reynolds number.

All in all, it is thus safe to conclude that very little is known about the flow of non-Newtonian fluids (even for purely viscous models) past an array of circular cylinders and the available information is limited only to the creeping region. Admittedly most polymeric solutions and melts display varying levels of shear thinning and viscoelastic characteristics. An ultimate analysis should therefore incorporate the role of both these rheological characteristics. It is, however, preferable to build up progressively the level of complexity, and therefore to keep the complexity at a tractable level, it is proposed to elucidate the role of shear thinning viscosity in this flow configuration. In addition, because the flow rate (and velocity) is usually small and the corresponding Deborah number would therefore be small, this suggests that the viscoelastic effects would be of secondary importance. This should further diminish with the increasing porosity of fibrous beds and the resistance to flow is primarily governed by shear viscosity under these circumstances. Therefore, this work should be seen as the first building block in the overall analysis. In this work, the equations of motion coupled with the cell model have been solved numerically to investigate the flow of power law fluids past (normal to) a collection of long cylinders. The Reynolds number of flow has been varied from 0.001 to 10, which is typical of applications in such porous media flows. In addition to the detailed kinemat-

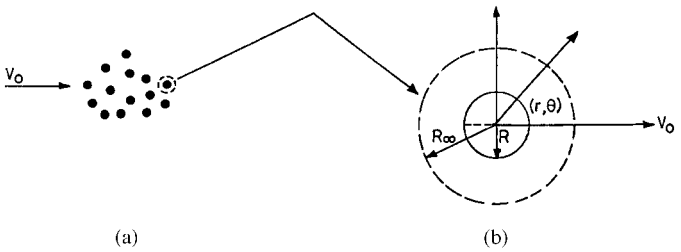

Figure 1 (a) Schematic representation of flow; (b) free surface cell model representation.

ics of flow, overall gross parameters such as flow resistance have been evaluated as a function of the pertinent physical and kinematic variables. The paper is concluded by presenting detailed comparisons with the previous scant theoretical as well as experimental results available in the literature.

PROBLEM STATEMENT AND IDEALIZATION

Consider the steady and axisymmetric incompressible flow of an inelastic power law fluid normal to an array of long cylinders as shown schematically in Figure 1a. Due to the axisymmetry, no flow variable depends upon the z coordinate and $V_z = 0$. In cylindrical coordinates, the equations of continuity, r- and θ- components of the momentum balance in dimensionless form, are written as[18]:

$$\frac{1}{r}\frac{\partial}{\partial r}(rV_r) + \frac{1}{r}\frac{\partial V_\theta}{\partial \theta} = 0 \tag{1}$$

r-component:

$$\frac{\partial V_r}{\partial t} + V_r\frac{\partial V_r}{\partial r} + \frac{V_\theta}{r}\frac{\partial V_r}{\partial \theta} - \frac{V_\theta^2}{r} = -\frac{1}{2}\frac{\partial p}{\partial r} + \frac{2^n}{\mathrm{Re}}\left[\frac{1}{r}\frac{\partial}{\partial r}(r\tau_{rr}) + \frac{1}{r}\frac{\partial \tau_{r\theta}}{\partial \theta} - \frac{\tau_{\theta\theta}}{r}\right] \tag{2}$$

θ-component:

$$\frac{\partial V_\theta}{r\partial t} + V_r\frac{\partial V_\theta}{\partial r} + \frac{V_\theta}{r}\frac{\partial V_\theta}{\partial \theta} + \frac{V_rV_\theta}{r} = -\frac{1}{2r}\frac{\partial p}{\partial \theta} + \frac{2^n}{\mathrm{Re}}\left[\frac{1}{r^2}\frac{\partial}{\partial r}(r^2\tau_{r\theta}) + \frac{1}{r}\frac{\partial \tau_{\theta\theta}}{\partial \theta}\right] \tag{3}$$

The rheological equation of state for a power law fluid is written as:

$$\tau_{ij} = 2\eta\varepsilon_{ij} \tag{4}$$

and

$$\eta = (2\Pi)^{(n-1)/2} \tag{5}$$

In eqs. (1) and (5), the velocity terms have been scaled using the faraway streaming velocity V_o, pressure has been scaled using $\frac{1}{2}\rho V_o^2$, radial distance using the radius of cylinder R, the extra stress components using $m(V_o/R)^n$, and the second invariant of the rate of deformation tensor II using $(V_o/R)^2$. It is written in terms of the velocity components as[18]:

$$\Pi = \varepsilon_{rr}^2 + \varepsilon_{\theta\theta}^2 + 2\varepsilon_{r\theta}^2 \tag{6}$$

where

$$\varepsilon_{rr} = \frac{\partial V_r}{\partial r}; \quad \varepsilon_{\theta\theta} = \frac{1}{r}\frac{\partial V_\theta}{\partial \theta} + \frac{V_r}{r} \text{ and } \varepsilon_{r\theta} = \frac{1}{2}\left[r\frac{\partial}{\partial r}\left(\frac{V_\theta}{r}\right) + \frac{1}{r}\frac{\partial V_r}{\partial \theta}\right] \tag{7}$$

By introducing a stream function ψ (scaled using V_oR), the two velocity components V_r and V_θ can be written as:

$$V_r = (1/r)(\partial\psi)/(\partial\theta) \tag{8a}$$

$$V_\theta = -(\partial\psi)/(\partial r) \tag{8b}$$

Similarly introducing the usual vorticity function ω(scaled as V_o/R) defined as:

$$\omega = -B^2\psi \tag{9}$$

where the differential operator $B^2 \equiv (\partial^2/\partial r^2 + 1/r\ \partial/\partial r + 1/r^2\ \partial^2/\partial\theta^2)$

Similarly, rewriting eq. (7) using eqs. (8) and (9) in terms of ψ and ω:

$$\Pi = (2/r^2)\left(\frac{\partial^2\Psi}{\partial r\partial\theta} - \frac{1}{r}\frac{\partial\psi}{\partial\theta}\right)^2 + 2\left(\frac{\partial^2\psi}{\partial r^2} + \frac{\omega}{2}\right)^2 \quad (10)$$

Now eliminating pressure between eq. (2) and eq. (3) by the usual method of cross-differentiation, i.e.,

$$\frac{\partial}{\partial\theta}\left(\frac{\partial p}{\partial r}\right) = \frac{\partial}{\partial r}\left(\frac{\partial p}{\partial\theta}\right) \quad (11)$$

and introducing the stream function ψ and the vorticity function ω, together with some rearrangement, it leads to:

$$\frac{\partial\omega}{\partial t} + \frac{1}{r}\left[\left(\frac{\partial\omega}{\partial r}\frac{\partial\psi}{\partial\theta}\right) - \left(\frac{\partial\omega}{\partial\theta}\frac{\partial\psi}{\partial r}\right)\right] = \frac{2^n\eta}{\mathrm{Re}}B^2\omega + \frac{2^{n+1}}{\mathrm{Re}}\left[\left(\frac{\partial\omega}{\partial r} + \frac{1}{2}\frac{\omega}{r} + \frac{1}{r}\frac{\partial^2\psi}{\partial r^2}\right)\frac{\partial\eta}{\partial r} + \frac{1}{r^2}\left(\frac{\partial\omega}{\partial\theta} - \frac{2}{r^2}\frac{\partial\psi}{\partial\theta} + \frac{2}{r}\frac{\partial^2\psi}{\partial r\partial\theta}\right)\frac{\partial\eta}{\partial\theta} - \left(\frac{\partial^2\psi}{\partial r^2} + \frac{\omega}{2}\right) \times \left(\frac{\partial^2\eta}{\partial r^2} - \frac{1}{r^2}\frac{\partial^2\eta}{\partial\theta^2}\right) + \frac{2}{r^2}\left(\frac{\partial^2\psi}{\partial r\partial\theta} - \frac{1}{r}\frac{\partial\psi}{\partial\theta}\right)\frac{\partial^2\eta}{\partial r\partial\theta}\right] \quad (12)$$

Equation (12) is the generalized form of the Navier-Stokes equation in terms of the stream function and vorticity for axisymmetric flow of power law fluids in polar coordinates. Note that even though the main thrust of the present work is on steady flow, the transient term has been retained in the momentum equation because the false transient technique was used to numerically solve these equations as discussed in a later section.

It is readily recognized that in addition to the field equations, a mathematical description of the inter-particle (cylinder-cylinder) interactions is also needed to complete the problem description. Amongst the various approaches available currently,[19,20] the so-called free surface cell model[19] has been shown to be moderately successful in predicting the macroscopic fluid flow phenomena in multiparticle systems, for example, flow resistance for both Newtonian and inelastic fluids in granular porous media,[21–25] sedimentation of clouds of fluid particles in quiescent power law fluids,[26,27] and of porous particles[28]. The range of applications shows the extremely versatile nature of this simple approach. Hence, in this study, the inter-cylinder interactions will be modelled using the free surface cylinder-in-cylinder model.

The free surface cell model[19] postulates each cylinder (of radius R) to be surrounded by a hypothetical concentric cylindrical envelope of fluid of radius R_∞ such that the porosity of each cell is equal to the mean voidage of the overall array. Furthermore, each of such cells is made a noninteracting type by imposing the boundary condition of zero shear stress on the cell boundary. This approach thus converts a difficult many-body problem into a conceptually much simpler one-body equivalent. The free surface cell model as applied to the present problem is shown in Figure 1b, together with the cylindrical coordinate system employed in this work.

The physically realistic boundary conditions thus now include the usual no-slip boundary condition on the surface of the cylinder, i.e.,

$$\text{At } r = 1 \quad V_r = 0 \quad \text{and} \quad V_\theta = 0 \quad (13a)$$

and cell boundary ($r = r_\infty$) is assumed to be frictionless, i.e.,

$$\text{At } r = R_\infty, \tau_{r\theta} = 0 \quad \text{and} \quad V_r = \cos\theta \quad (13b)$$

However, since the governing differential eq. (12) has been written in terms of ψ and ω, eqs. (13a) and (13b) need to be expressed in terms of these variables. This transformation leads to the following equivalent boundary conditions that were actually used in the present numerical work:

On the cylinder surface ($r = 1$):

$$\cdot\ \omega = -\frac{\partial^2\psi}{\partial r^2} \quad \text{and} \quad \psi = 0 \quad (14a)$$

On the cell surface ($r = r_\infty$):

$$\cdot\ \psi = r_\infty \sin\theta \quad (14b)$$

$$\cdot\ \omega = -\frac{2}{r_\infty}\left(\frac{\partial\psi}{\partial r} - \sin\theta\right) \quad (14c)$$

where the dimensionless cell radius $r_\infty = R_\infty/R$ is related to the voidage of the array ϵ as:

$$r_\infty = (1 - \varepsilon)^{-1/2} \quad (15)$$

Clearly, as the value of cell radius increases, i.e., the concentration of cylinders decreases (voidage increases) and when it decreases, the value of voidage decreases. Thus, by simply varying the value of r_∞, different values of voidage of the array can be accomplished.

In addition to the boundary conditions outlined in eqs. (14a–c) the condition of symmetry was imposed by satisfying $\psi = 0$ and $\omega = 0$ at $\theta = 0$ and $\theta = \pi$ planes.

Thus, eqs. (5), (8),(10), and (12) subject to the conditions outlined in eqs. (13) and (14), together with the symmetry condition at $\theta = 0$ and $\theta = \pi$ lines provide the theoretical framework for mapping out the flow domain ($1 \le r \le r_\infty$; $\pi > \theta > 0$) in terms of the ψ, ω and η as functions of r and θ. These results, in turn, can be processed further to evaluate the components of the fluid drag exerted on the cylinder using the following expressions:

$$C_{DP} = \frac{1}{2}\int_0^{2\pi} p_{r=1} \cos\,\theta\, d\theta \tag{16a}$$

$$C_{DF} = \frac{2^n}{\mathrm{Re}}\int_o^{2\pi} (\eta\omega)_{r=1} \sin\,\theta\, d\theta \tag{16b}$$

where the C_{DP} and C_{DF} are the contributions due to pressure and friction, respectively. The total drag coefficient C_D is simply the sum of these two contributions and is related to the drag force F_D per unit length of the cylinder as follows:

$$C_D = C_{DP} + C_{DF} = \frac{2F_D}{\rho V_0^2 d} \tag{17}$$

where d is the cylinder diameter.

It is seen from eq. (16b) that the value of the integrand is known as the solution is being sought in terms of the viscosity and vorticity and hence the evaluation of C_{DF} poses no difficulty. On the other hand, the estimation of the pressure contribution, C_{DP}, necessitates a knowledge of the pressure on the surface of the cylinder and it was calculated as follows. The r-component of the momentum balance (eq. 2) can be integrated with respect to r (for $\theta = 0$) from r = 1 to $r = r_\infty$ to get:

$$p_0|_{\theta=0} = (1 - V_r^2) + (2^{n+2}/\mathrm{Re})\int_1^{r_\infty}\left(\frac{\eta}{2r}\frac{\partial\omega}{\partial\theta} - \frac{\partial V_r}{\partial r}\cdot\frac{\partial\eta}{\partial r}\right)_{\theta=0} dr \tag{18}$$

and the stagnation pressure at the front stagnation point is obtained by substituting $V_r = 0$ in eq. (18):

$$p_0 = 1 + \left(\frac{2^{n+2}}{\mathrm{Re}}\right)\int_1^{r_\infty}\left(\frac{\eta}{2r}\frac{\partial\omega}{\partial\theta} - \frac{\partial V_r}{\partial r}\cdot\frac{\partial\eta}{\partial r}\right)_{\theta=0} dr \tag{19}$$

Now the pressure distribution on the surface of the cylinder (r =1) can be written in terms of p_o as:

$$p|_{r=1} = p_0 + \frac{2^{n+1}}{\mathrm{Re}}\int_0^{\theta}\frac{\partial(\eta\omega)}{\partial r}|_{r=1}\, d\theta \tag{20}$$

Because the values of p_o, η, and ω are known on the surface of the cylinder, eq. (20) yields the value of $p|_{r=1}$ that can now be substituted in eq. (16a) to evaluate the pressure drag coefficient C_{DP}.

In summary, therefore, once the values of η, ψ, and ω are known in the flow domain, one can evaluate the dimensionless resistance to flow in terms of the individual and total drag coefficients. The numerical solution procedure to solve the field equations to generate the point values of n, ψ, and ω is described briefly in the next section.

NUMERICAL SOLUTION PROCEDURE

The governing equations, namely the vorticity and stream function eqs. (9 and 12), along with the power-law viscosity eqs. (5 and 6), have been solved by a finite difference scheme using the false transient time-stepping method to obtain the steady-state solution. For each time-step, new values of vorticity are obtained using an implicit time-stepping scheme, whereas the corresponding compatible values of the stream function are then obtained using the Gauss-Siedel iterative method. These in turn permit the evaluation of the corresponding viscosity values. This procedure is repeated time-step after time-step until the steady solution is reached. The time-stepping was continued till the maximum change in the value of stream function between two successive time-steps was less than 10^{-10}. Sometimes an under-relaxation factor of 0.5 was used in the Gauss-Siedel iteration to achieve the desired level of convergence. An implicit first order upwind

Table I Comparison Between Analytical and Numerical Results for $n = 1$ at Re = 0.01

	Analytical	Numerical
$\varepsilon = 0.4$		
C_{DP}	95528.72	95497.05
C_{DF}	29393.47	29397.50
C_D	124922.19	124894.55
$\varepsilon = 0.5$		
C_{DP}	37749.4	37721.47
C_{DF}	16182.10	16186.32
C_D	53931.51	53907.80
$\varepsilon = 0.7$		
C_{DP}	7932.824	7921.92
C_{DF}	5684.275	5698.03
C_D	13617.099	13619.95
$\varepsilon = 0.9$		
C_{DP}	1938.11	1934.94
C_{DF}	1862.28	1863.26
C_D	3800.39	3798.20

scheme was used to discretize the convective terms for low Reynolds number situations (Re $<\sim 0.1$) and the explicit QUICK scheme was used for higher values of the Reynolds number. The Laplacian terms were discretized using the usual center-difference scheme.

Because a finer grid is needed at and near the boundaries to preserve reasonable levels of accuracy, a nonuniform grid was used. Such a grid was generated using an exponential function to generate half of the radial points, i.e., $r_I = \exp[k(I-1)]$. I=1,2,. . . N/2, and then reflecting them around the midpoint to complete the other half. Uniform intervals in the θ-direction were used.

For the values of the bed porosity smaller than 0.7, 401 × 41 grid points were used in the radial and angular directions respectively. For $\epsilon > 0.7$, a 501 × 51 grid was used. All results reported herein have been checked for mesh independence by using at least two different meshes.

In broad terms, as the value of the power law index decreased below the value of unity, it became progressively more difficult to achieve the required level of convergence, especially for the values of $n \leq 0.3$. However in each case the convergence criterion, applied for the stream function evaluation by the Gauss-Siedel method, was $\Delta\psi/\psi < 10^{-4}$ and the overall criterion of 10^{-10} was employed. Only those values of drag coefficient which had stabilized up to 3–4 significant digits were accepted. More details regarding the numerical solution procedure are available in another recent study.[17]

RESULTS AND DISCUSSION

In this work, the governing equations have been solved numerically to obtain detailed information on the streamline and iso-vorticity lines, surface viscosity distribution as well as on the resistance to flow in terms of nondimensional drag coefficient for a range of values of the physical and kinematic variables as: $0.4 \leq n \leq 1$; $0.4 \leq \epsilon \leq 0.95$ and $0.01 < Re < 10$. At the outset, it is, however, appropriate to validate the numerical solution procedure and the choice of numerical parameters such as the convergence criteria, mesh size, under-relaxation factor, and so on as this will help establish the accuracy of the new results for power law fluids obtained in this study.

Validation of Numerical Solution Procedure

Because an analytical solution of the governing equations is available for the flow of Newtonian fluids ($n = 1$) at very low Reynolds number ($\rightarrow 0$) which is given by[17,19]:

$$\psi = (Cr^3 + Dr \ln r + Er + F/r)\sin\theta \quad (21)$$

where the four unknown coefficient C,D,E,F are evaluated by applying the boundary conditions outlined in eqs. (13a) and (13b) as:

Table II Values of Drag Coefficient as a Function of ε and n at Re = 0.01

	$n = 0.9$	$n = 0.8$	$n = 0.6$	$n = 0.5$
$\varepsilon = 0.4$				
C_{DP}	64507.19	41910.93	20338.71	11978.97
C_{DF}	19694.92	12681.40	5993.97	3825.17
C_D	84202.12	54592.33	26332.68	15804.15
$\varepsilon = 0.5$				
C_{DP}	27472.53	20005.74	10506.74	7112.79
C_{DF}	11607.31	8309.85	4217.63	2931.69
C_D	39079.84	28315.60	14724.20	10044.48
$\varepsilon = 0.7$				
C_{DP}	6475.68	5386.61	3610.44	2527.65
C_{DF}	4490.88	3644.10	2295.37	1619.25
C_D	10966.56	9030.71	5905.82	4146.90
$\varepsilon = 0.9$				
C_{DP}	1832.55	1735.55	1540.15	1355.48
C_{DF}	1689.81	1539.75	1237.71	1067.94
C_D	3522.36	3275.31	2777.86	2423.42
$\varepsilon = 0.95$				
C_{DP}	1279.89	1259.85	1168.03	1120.84
C_{DF}	1181.25	1116.48	941.74	888.85
C_D	2461.14	2376.33	2109.71	2009.69

Table III Effect of Reynolds Number on Drag Coefficient

		$n = 1.0$	$n = 0.8$	$n = 0.6$	$n = 0.5$
$\varepsilon = 0.5$					
	C_{DP}	1618.53	825.87	381.60	275.36
R = 0.1	C_{DF}	3775.05	1997.78	950.19	605.48
	C_D	5393.58	2823.65	1331.79	880.84
	C_{DP}	161.99	82.55	39.14	26.90
1	C_{DF}	378.55	199.39	89.68	56.52
	C_D	540.54	281.93	128.82	83.42
	C_{DP}	32.61	16.72	7.46	5.41
5	C_{DF}	77.91	42.6	19.93	12.28
	C_D	110.52	59.32	27.39	17.69
	C_{DP}	16.55	8.67	4.03	2.75
10	C_{DF}	41.42	24.27	11.49	7.06
	C_D	57.97	32.93	15.52	9.81
$\varepsilon = 0.9$					
	C_{DP}	186.46	147.24	108.35	89.11
0.1	C_{DF}	194.05	174.15	135.55	113.17
	C_D	380.51	321.39	243.89	202.29
	C_{DP}	18.88	14.69	11.10	9.04
1	C_{DF}	20.00	18.16	14.21	11.84
	C_D	38.88	32.85	25.31	20.88
	C_{DP}	4.435	3.35	2.44	1.84
5	C_{DF}	5.44	5.06	3.86	2.97
	C_D	9.875	8.41	6.30	4.81
	C_{DP}	2.58	1.935	1.34	1.12
10	C_{DF}	3.83	3.620	2.61	1.99
	C_D	6.41	5.555	3.95	3.11

$$C = -\frac{D}{2(1 - r_\infty^4)} \tag{22a}$$

$$D = \frac{2(1 + r_\infty^4)}{2(1 + r_\infty^4)\ln r_\infty - r_\infty^4 + 1} \tag{22b}$$

$$E = \frac{D(1 - r_\infty^4)}{2(1 + r_\infty^4)} \tag{22c}$$

$$F = \frac{Dr_\infty^4}{2(1 + r_\infty^4)} \tag{22d}$$

where r_∞, in turn, is related to the voidage via eq. (15). Based on the stream function given by eq. (21), the vorticity, friction, pressure, and total drag coefficient respectively are given by:

$$\omega = -(8\ \mathrm{Cr} + (2D/r))\sin\theta \tag{23}$$

$$C_{DF} = \frac{2\pi(8C + 2D)}{\mathrm{Re}} \tag{24}$$

$$C_{DP} = -\frac{2\pi(8C - 2D)}{\mathrm{Re}} \tag{25}$$

and

$$C_D = C_{DF} + C_{DP} = (8\pi D/\mathrm{Re}) \tag{26}$$

Hence, for a known value of voidage, i.e., ϵ or r_∞, one can readily evaluate the values of the individual and total drag coefficients using eqs. (24) to (26). A comparison between the present numerical and analytical values of C_{DP}, C_{DF},and C_D for a few values of voidage at Re = 0.01 is shown in Table I. An examination of this table shows that the analytical and numerical values of the drag coefficients are within 0.2% of each other. Simi-

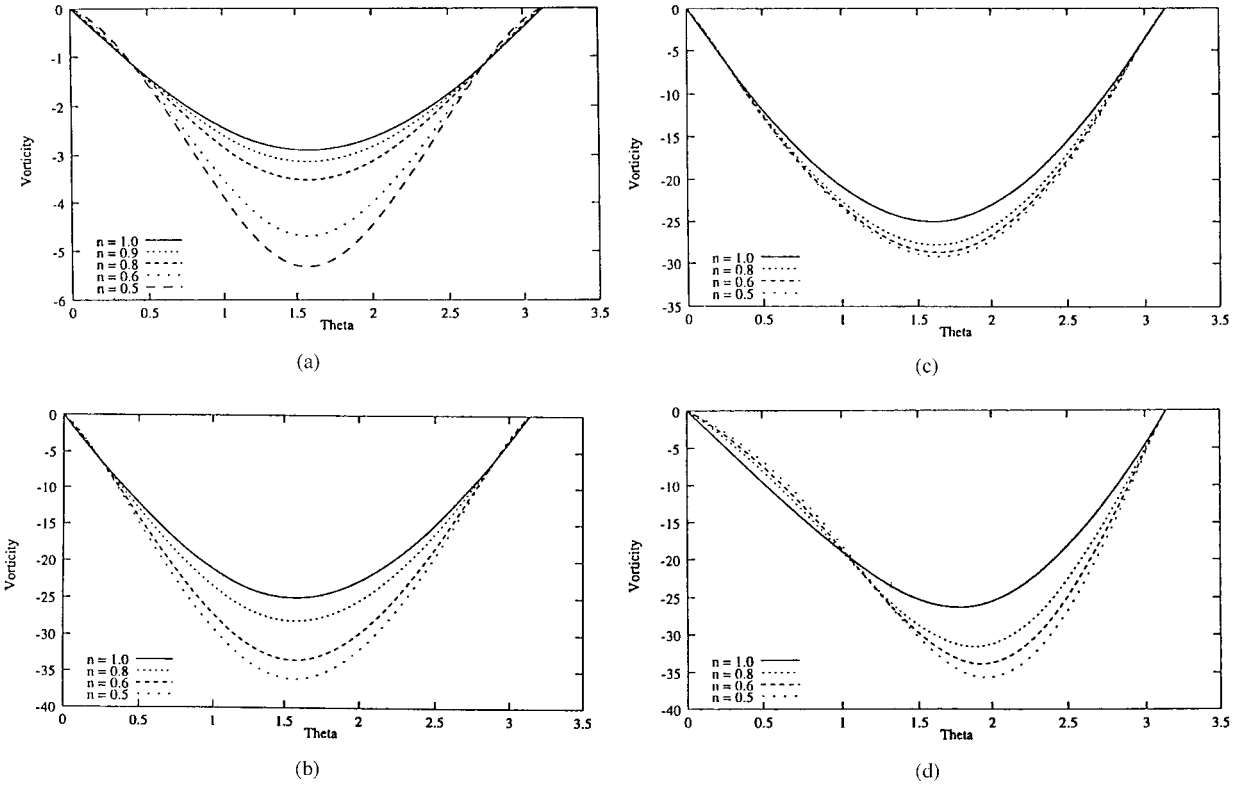

Figure 2 Surface vorticity plots. (a) Re = 0.01, $\epsilon = 0.9$; (b) Re = 0.01, $\epsilon = 0.5$; (c) Re = 1, $\epsilon = 0.5$; (d) Re = 10, $\epsilon = 0.5$

larly close results were also obtained for the other values of voidage. In addition, a few results were obtained at Re = 0.001 and these values clearly revealed that C_D varies as 1/Re in this region and that Re = 0.01 is appropriate for investigating the so-called creeping flow region. Aside from these comparisons of integral quantities, extensive detailed comparison between the analytical and numerical values of ψ and ω were also made in the entire flow domain $1 \leq r \leq r_\infty$ and the discrepancy between the analytical and numerical values seldom exceeded 0.1–0.15% thereby lending further support to the reliability and accuracy of the numerical solution procedure used in this study. Similar comparisons between the present results and those available in the literature at Re = 10 revealed the two values to be within 0.2% of each other thereby providing another independent validation of the present results.

Based on the aforementioned comparisons and our previous experience,[25] it is perhaps fair to say that the new results for power law fluids presented in the ensuing sections are accurate to within 0.5–1%.

Results for Power Law Fluids

As mentioned earlier, extensive numerical results on the individual and total drag coefficients as well as on the detailed kinematics in terms of the values of the surface vorticity, viscosity variation on the cylinder surface, and streamline plots have been obtained, and these are presented and discussed in the next section.

Drag coefficient

The values of C_{DP}, C_{DF}, and C_D were calculated in the following ranges of variables : $0.4 \leq \epsilon \leq 0.95$; $1 > n > 0.4$ and for Re = 0.01, 0.1, 1, 5, and 10. The values for Re = 0.01 relating to the so-called creeping flow region are summarized in Table II. An inspection of this table suggests that, for a fixed value of porosity (ϵ), the values of the individual as well as total drag coefficients decrease below their value for Newtonian fluids with increasing degree of shear thinning behavior, i.e., the lower the value of n, the lower is the resistance to flow of the fluid. This is mainly due to the fact that a major part of the surface of the solid

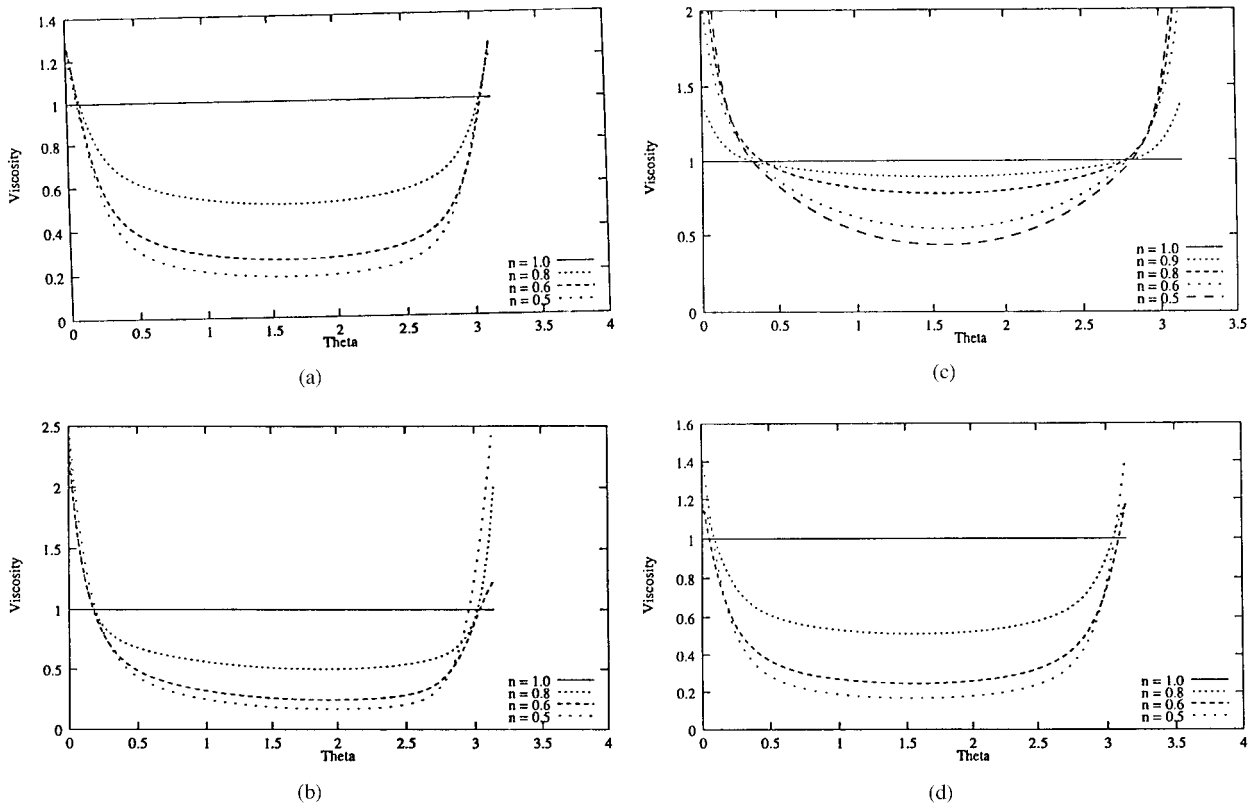

Figure 3 Viscosity variation on the surface. (a) Re = 0.01, ϵ = 0.9; (b) Re = 0.01, ϵ = 0.5; (c) Re = 1, ϵ = 0.5; (d) Re = 10, ϵ = 0.5.

cylinders is exposed to an effective viscosity that is lower than that in the case of a Newtonian fluid. Because the viscous forces in creeping flow region are in equilibrium with the pressure forces, both contributions to drag decrease with the lowering of the power law index. Similarly, for a fixed value of n, as expected the values of drag coefficient decrease rapidly with the increasing porosity that can be directly attributed to smaller velocity gradients than those present in dense systems. The intricate interplay between the role of ϵ and n on drag coefficient is further elucidated by examining the ratio C_{DP}/C_{DF} as a function of ϵ for a range of values of n. It is clearly seen that in dense systems this ratio hovers around $\sim$ 3-3.5 whereas it drops to about 1 at ϵ = 0.9 and the flow behavior index exerts little influence on it. These dependencies are qualitatively similarly to those observed for the flow of power law fluids in granular beds of spherical particles.[22–25]

The results summarized in Table III elucidate the role of increasing inertial effects on the value of drag coefficient for a range of values of n, but only for two values of porosity, namely, ϵ = 0.5 and ϵ = 0.9. It is clearly seen that the effect of both the Reynolds number and the power law index are much more prominent in more dense packing of ϵ = 0.5 than that in the case of ϵ = 0.9. For instance, for the case of a fixed value of ϵ = 0.5, the value of drag coefficient varies nearly by a factor of 6 as the value of n changes from 1 to 0.5, the corresponding range of variation is only about 2 for ϵ = 0.9. This is again attributable to lower rate of deformation of fluid elements in sparse systems. Some further insights into the nature of flow can be gained from the iso-vorticity, streamlines, and viscosity plots on the cylinder presented in the next section.

Surface vorticity, viscosity variation on the surface of the solid cylinder, and streamline plots

The effects of voidage, Reynolds number, and the flow behavior index on the value of the dimensionless surface vorticity are shown in Figures 2a–d. An inspection of these figures reveals that the surface vorticity is negative on the cylinder surface and it displays perfect fore- and aft-symme-

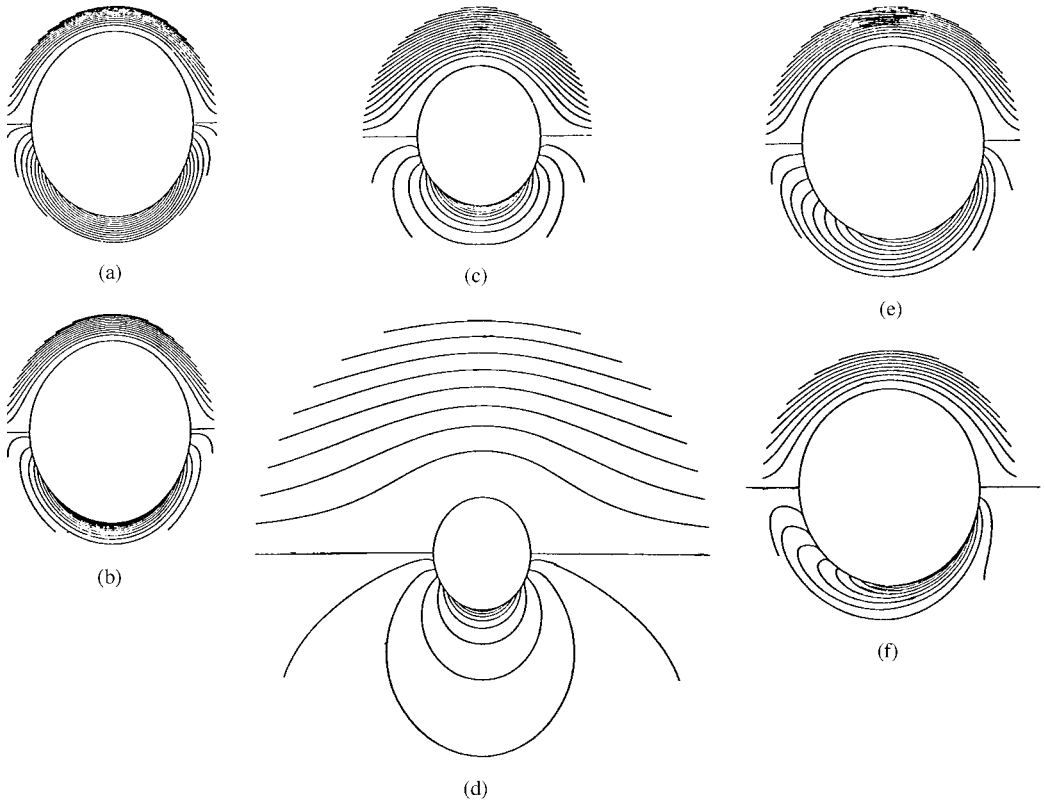

Figure 4 Iso-vorticity (bottom half) and streamline plots (top half). (a) Re = 0.01, n = 1, ϵ = 0.4; (b) Re = 0.01, n = 0.5, ϵ = 0.4; (c) Re = 0.01, n = 0.5, ϵ = 0.4; (d) Re = 0.01, n = 0.5, ϵ = 0.4; (e) Re = 0.01, n = 0.5, ϵ = 0.4; (f) Re = 10, n = 0.5, ϵ = 0.4.

try up to about Re $\sim$ 1 and a clear asymmetry sets in at Re = 10, as seen in Figure 2d. Furthermore, for a given value of the Reynolds number and porosity, the magnitude of the surface vorticity increases with the increasing degree of non-Newtonian behavior. Such plots can facilitate the estimation of the flow separation angle. In present case, the Reynolds number of flow is, however, not sufficiently high for flow separation to occur.

Figures 3a–d show the variation of the dimensionless viscosity on the cylinder surface for a range of combinations of porosity, Reynolds number, and power law index. An examination of these figures shows that excepting small regions near the front and rear stagnation points, the surface of the cylinder is in contact with a fluid of apparent viscosity that is not only lower than that in the case of a Newtonian fluid but is also uniform over the surface of the cylinder, at least in concentrated systems. This is in part responsible for the lowering of the flow resistance in shear thinning fluids. However, the region exposed to uniform viscosity progressively reduces as the porosity increases, and similarly, the variation becomes increasingly skewed as the Reynolds number of flow increases.

Finally, representative streamline and constant vorticity lines are shown in Figure 4a–e for a range of combination of ϵ, Re, and n. Qualitatively these patterns are similar to those observed for Newtonian fluids and the main features can be summarized as follows: Up to about Re $\sim$ 1, the stream lines and constant vorticity lines display complete fore- and aft- symmetry thereby confirming the existence of the so-called creeping or viscous flow. However, the lower the voidage, the higher the Reynolds number up to which this symmetry prevails. This is consistent with the drag results reported herein as well as those reported previously for granular beds of spheres. As the value of the Reynolds number increases, the above-said symmetry is progressively destroyed. The lower values of n also result in the destruction of the symmetry in flow field; this is presumably so due to the lower effective viscosity of the fluid.

Table IV Comparison Between the Present and Previous Approximate Analytical Results[16] (In Terms of $\Lambda = C_D$ Re) for Re = 0.01

	ε = 0.4		0.5		0.7		ϵ = 0.9	
	Present	Ref. 16*	Present	Ref. 16*	Present	Ref. 16	Present	Ref. 16*
n = 1	1248.95	1248.93	539.08	539.13	136.23	136.60	37.89	37.90
n = 0.9	842.02	858.4	390.80	386.50	109.66	111.46	35.22	35.31
n = 0.8	545.92	567.70	283.15	284.53	90.30	90.89	32.75	33.05
n = 0.6	263.33	267.30	147.24	150.31	59.06	60.76	27.78	28.75
n = 0.5	158.04	173.67	100.44	108.92	41.47	48.63	24.23	26.30

* Arithmetic mean of upper and lower bounds.

Comparison with Previous Analytical and Experimental Results

As mentioned previously, there is only one analytical study available for the creeping flow of power law fluids within the framework of the free surface cell model. In this analytical study, approximate upper and lower bounds were obtained. It is thus appropriate to compare these results with the present numerical results that are regarded as being more accurate and reliable. Such a comparison is shown in Table IV. Excellent agreement between the two is seen to exist, though the divergence between the two values increases as the value of n drops below unity, reaching about 10% for n = 0.5, and it is likely to increase further for values of n < 0.5. However, the upper and lower bound results are restricted to the creeping flow only. Furthermore, there appears to be a trend that the present numerical results are close to the upper bound for weakly shear thinning behavior, and these progressively move towards the lower bound as the value of n drops further.

The only other theoretical work is the numerical study of Skartsis et al.[15] who studied the creeping flow of power law fluids through square and staggered configurations and reported numerical values of flow resistance for two values of porosity, namely, ϵ = 0.43 and 0.68. It is not possible to recalculate their results in the form required here, but the present results can be expressed in terms of the so-called Kozeny constant k^*, defined by them as follows:

$$k^* = \frac{\varepsilon^{2n+1}}{(1-\varepsilon)^n}\left(\frac{n}{6n+2}\right)^n\left(\frac{C_D\,\mathrm{Re}}{\pi}\right) \qquad (27)$$

At the outset, it is useful to perform a detailed comparison between the predictions and experimental data available in the literature for n = 1.

Figure 5 compares the values of the Kozeny constant k as predicted by the present analysis and the experimental values derived from the flow in fibrous beds as compiled in the literature.[13,14] Excellent agreement is seen to exist between the present analysis and the experimental results. Similarly, several other empirical expressions[29–32] are available in the literature to represent the flow resistance for the creeping flow of Newtonian fluids in fibrous beds. These have been re-cast in terms of the Kozeny constant and are presented here in Table V; The present numerical predictions (n = 1 and Re = 0.01) are contrasted in Table VI with the values calculated using the expressions listed in Table V. Bearing in mind the extent of experimental scatter as reflected in the diverse predictions, an examination of this table clearly shows excellent agreement between these voluminous experimental results (represented via the empirical correlations for k) and the present

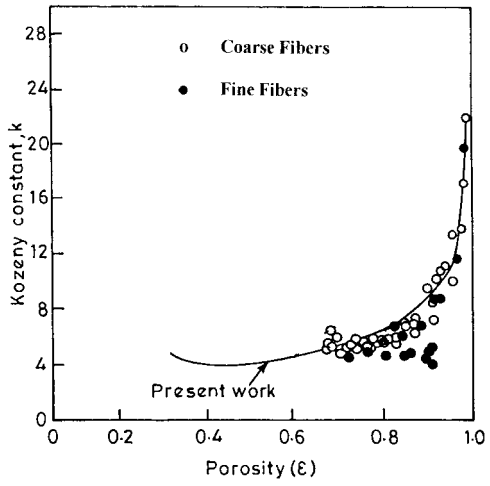

Figure 5 Comparison of present results with experimental results for fibrous beds (n = 1, Re = 0.01).

Table V Empirical Expressions for k as Function of ε

Reference	Expression for k	Remarks
Davies[29]	$\frac{4\varepsilon^3}{(1-\varepsilon)^{1/2}}\{1 + 56(1 - \varepsilon)^3\}$	$\varepsilon < 0.98$
	$\frac{4.4\varepsilon^3}{(1-\varepsilon)^{1/2}}\{1 + 56(1 - \varepsilon)^3\}$	$\varepsilon > 0.98$
Carroll (as cited by Han[30])	$5 + \exp\{14(\varepsilon - 0.8)\}$	—
Ingmanson et al.[31]	$3.5\frac{\varepsilon^3}{(1-\varepsilon)^{1/2}}\{1 + 57(1 - \varepsilon)^3\}$	—
Chen[32]	$0.484\left(\frac{\varepsilon^3}{1-\varepsilon}\right)\left\{\ln\frac{0.64}{(1-\varepsilon)^{1/2}}\right\}^{-1}$	$\varepsilon > 0.7$

numerical predictions. Finally, we report on another comparison between the experimental values of the permeability of nylon and aluminium rod assemblies for a Newtonian glucose solution with the present predictions, and this is shown in Table VII. An examination of this table again reveals fair correspondence between the experimental and predicted values. From the aforementioned extensive comparisons, it is evident that the simple cell model employed herein has been moderately successful in predicting the resistance to the flow of Newtonian fluids in a variety of fibrous media. It is thus a fair expectation that this approach is likely to yield acceptable results for power law fluids as well. In most analogous studies pertaining to non-Newtonian fluids, some of the data available in the literature have been obtained using test media that were not always checked for possible viscoelastic effects whereas some exclusively dealt with highly viscoelastic media. Thus it is not appropriate to compare them with the present predictions where the viscoelastic effects have been neglected altogether. However, three of the test fluids used by Skartsis et al.[15] were shown to have very small values of the fluid relaxation time. This coupled with the low value of the Reynolds number (or flow velocity) will make the corresponding Deborah number very small and viscoelastic effects must be negligible under these conditions. A comparison between their experimental values and the present numerical values of k^* is shown in Table VIII where good correspondence is seen to exist between the two values, although the experimental values are consistently higher than the predicted values of k^*. This can safely be ascribed to the small degree of viscoelasticity present in the test fluids and to possible wall effects inherent in experimental results.

On the other hand, Adams and Bell[6] and Prakash et al.[7] have reported experimental values of pressure drop for the flow of polymer solutions normal to cylinders arranged in a range of configurations thereby varying ϵ in the range 0.4 to 0.6 and a generalized Reynolds number in the range ~1 to 1000. Prakash et al.[7] reconciled most of the data and put forward the following single

Table VI Comparison Between the Present Values and Empirical Expressions for k (listed in Table V) for Re ≤ 0.1

$\varepsilon \rightarrow$	0.5	0.6	0.7	0.9	0.95	0.99
k						
Davies[29]	5.65	6.26	6.30	9.74	15.44	42.7
Chen[32]	—	—	5.07	5.56	8.30	25.55
Carroll (as cited in ref. 30)	5.01	5.06	5.25	9.05	13.16	19.3
Ingmanson et al.[31]	5.02	5.56	5.56	8.53	13.52	34.0
Present work	5.36	5.62	6.19	11.01	17.14	53.8

Table VII Comparison Between the Present Predictions and Experimental Values of Permeability K/d^2 Sadiq et al.[33]

	Value of K/d^2	
ε	Experimental	Present Value
	Nylon rods	
0.388	7.5×10^{-4}	1.4×10^{-3}
0.49	3.05×10^{-3}	3.87×10^{-3}
0.592	9.67×10^{-3}	9.9×10^{-3}
	Aluminium Rods	
0.417	1.3×10^{-3}	1.9×10^{-3}
0.514	3.88×10^{-3}	4.8×10^{-3}
0.611	9.95×10^{-3}	11.7×10^{-3}

equation for both Newtonian and power law fluids:

$$f' = (130/\mathrm{Re}') + 0.7 \tag{28}$$

where

$$Re' = \mathrm{Re}\, F(n, \varepsilon)$$

$$F(n, \varepsilon) = \{((2n + 1)/3n)^n (12(1 - \varepsilon)/\varepsilon^2)^{n-1} (1 - \varepsilon)\}^{-1}$$

and

$$f' = (2C_D\varepsilon^3)/\pi$$

A comparison between the predictions of eq. (28) and the present results for $\epsilon = 0.4$, 0.5, and 0.7 is shown in Figure 6. An examination of this figure clearly shows that while there is no discernable trend present with regard to the value of n and that the present results show qualitatively similar dependence on Reynolds number as suggested by equation (28); however, equation (28) is seen to consistently over-predict the present results by about 30-40% which is comparable to the uncertainty of 25-30% inherent in equation (28) and ascertained from the comparisons reported by Prakash et al[7]. Furthermore, it is fair to add here that considerable confusion exists in the literature regarding the numerical constants of 130 and 0.7 in equation (28). For instance, in another study concerning the flow of Newtonian fluids across an hexagonal array of cylinders, Dybbs and Edwards[34] reported a equation similar to equation (28), but with the numerical constants of 96 and 1.75 respectively. For the sake of comparison, the predictions of their equation, i.e.,

$$f' = 96/\mathrm{Re}' + 1.75 \tag{29}$$

are also included in Figure 6 and the present results are seen to be much closer to eq. (29) than to the predictions of eq. (28). Furthermore, in assessing the comparison shown in Figure 6, the following factors must be borne in mind: the predictions are based on the assumption of long cylinders (L/R $\rightarrow \infty$) whereas in most experimental study, this ratio is of the order of 15–20. Wall effects have been neglected altogether in the analysis whereas the experimental results invariably entail a contribution from wall effects. Finally, considering the complexity of the flow geometry coupled with the simplicity and highly idealized nature of the model, the correspondence seen in Figure 6 is believed to be acceptable and satisfactory, at least for process engineering calculations standpoint.

CONCLUSIONS

In this work, the steady cross-flow of power law liquids at low to moderate Reynolds numbers past an assemblage of infinitely long cylinders has been studied to capture some features of non-Newtonian fluid flow in fibrous media. The hydrodynamic interactions between cylinders have been simulated using a simple cylinder-in-cylinder cell model. The governing equations have been solved numerically using the finite difference method. Extensive theoretical results encompassing wide ranges of Reynolds number ($0.01 \leq \mathrm{Re} \leq 10$), bed voidage ($0.4 \leq \epsilon \leq 0.95$) and the power law index ($1 \geq n \geq 0.4$) are presented and discussed herein. Detailed comparisons with the analytical results for the flow of Newtonian

Table VIII Comparison Between the Experimental and Predicted Values of k^* for Power Law Fluids

ε	n	k^*	
		Experimental	Present Theory
0.43–0.68	0.33	4.12–4.5	4.2
0.43–0.455	0.40	5.75	4.3

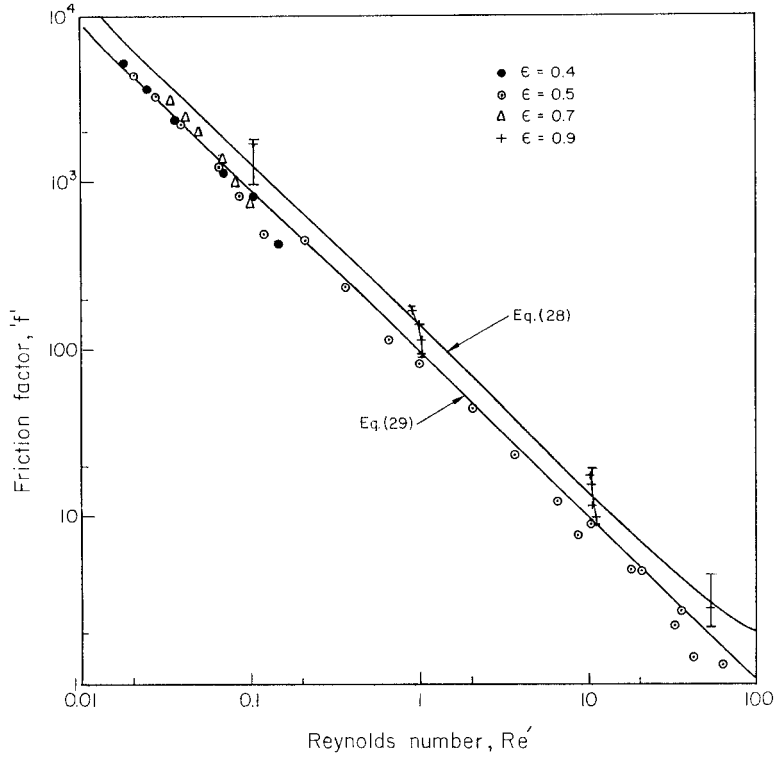

Figure 6 Comparison of present results with eqs. (28) and (29).

fluids at low Reynolds number suggest that the present numerical results are accurate to within 0.4%. Based on an extensive analysis of drag results and the detailed streamline patterns, the creeping flow region is believed to persist up to about the value of Re ~ 1. The total drag coefficient draws varying proportions of contributions from pressure and friction drag coefficients depending upon the values of n, ϵ, and Re, thereby indicating complex interplay between the fluid characteristics, bed structure, and kinematics of flow.

The extensive comparisons with the experimental results available in the literature lend further support to the validity of the theoretical results reported herein. The preliminary comparisons are affirmative and encouraging, at least in the range of $\sim 0.4 \leq \epsilon \leq \sim 0.7$.

NOMENCLATURE

C_D	drag coefficient (-)
C_{DF}	friction drag coefficient (-)
C_{DP}	pressure drag coefficient (-)
d	cylinder diameter (m)
F_D	drag force (N)
f	friction factor (-)
k^*	Kozeny constant (-)
m	power-law consistency ($Pa.s^n$)
n	power-law index (-)
p	pressure (Pa)
r	radial coordinate (m)
r_∞	dimensionless cell radius (-)
R	cylinder radius (m)
R_∞	cell radius (m)
Re	Reynolds number (-)
Re'	modified Reynolds number (-)
V_r, V_θ	component of velocity (m/s)
V_o	superficial velocity (m/s)

GREEK LETTERS

ϵ	bed voidage (-)
ϵ_{ij}	components of the rate-of-deformation tensor (s^{-1})
η	viscosity (Pa.s)
ρ	fluid density (kg/m^3)
τ_{ij}	components of extra stress tensor (Pa)
ψ	stream function (m^2/s)
ω	vorticity (s^{-1})
2II	second invariant of the rate-of-deformation tensor (s^{-2})

REFERENCES

1. Williams, J. G.; Morris, C. E. M.; Ennis, B. Polym Eng Sci 1974, 14, 413.
2. Springer, G. S. J Composite Mat 1982, 16, 400.
3. Astrom, B. T.; Pipes, R. B.; Advani, S. G. J Composite Mat 1992, 26, 1351.
4. Kiljanski, T.; Dziubinski, M. Chem Eng Sci 1996, 51, 4533.
5. Sorbie, K. S. Polymer Improved Oil Recovery; Blackie; Glasgow, 1992.
6. Adams, D.; Bell, K. J. Chem Eng Prog Sym Ser 1968, 64, (No.82), 133.
7. Prakash, O.; Gupta, S. N.; Mishra, P. Ind Eng Chem Res 1987, 26, 1365.
8. Ghosh, U. K.; Upadhyay, S. N.; Chhabra, R. P. Adv Heat Transf 1994, 24, 253.
9. Vossoughi, S.; Seyer, F. A. Can J Chem Eng 1974, 52, 666.
10. Chmielewski, C.; Petty, C. A.; Jayaraman, K. J Non-Newt Fluid Mech 1990, 35, 309.
11. Barboza, M.; Rangel, C.; Mena, B. J Appl Polym Sci 1979, 23, 281.
12. Chhabra, R. P. Bubbles, Drops and Particles in non-Newtonian Fluids; CRC Press; Boca Raton, FL, 1993.
13. Skartsis, L.; Kardos, J. L.; Khomami, B. Polym Eng Sci 1992, 32, 221.
14. Tripathi, A.; Chhabra, R. P. Chem Engng Commun 1996, 147, 197.
15. Skartsis, L.; Khomami, B.; Kardos, J. L.J Rheol 1992, 36, 589.
16. Tripathi, A.; Chhabra, R. P. Ind Eng Chem Res 1992, 31, 2754.
17. Satheesh, V. K.; Chhabra, R. P.; Eswaran, V. Can J Chem Eng 1999, 77, 978.
18. Bird, R. B.; Stewart, W. E.; Lightfoot, E. N. Transport Phenomena; John Wiley & Sons, Inc.; New York, 1960.
19. Happel, J. AIChEJ 1959, 5, 174.
20. Kuwabara, S. J Phys Soc Jpn 1959, 14, 527.
21. Chhabra, R. P.; Raman, J. R. Chem Eng Commun 1984, 27, 23.
22. Jaiswal, A. K.; Sundararajan, T.; Chhabra, R. P. Can J Chem Eng 1991, 69, 1235.
23. Jaiswal, A. K.; Sundararajan, T.; Chhabra, R. P. Int J Engng Sci 1991, 29, 693.
24. Jaiswal, A. K.; Sundararajan, T.; Chhabra, R. P. Int J Engng Sci 1993, 31, 293.
25. Jaiswal, A. K.; Sundararajan, T.; Chhabra, R. P. Num. Heat Transf 1992, 21A, 275.
26. Gummalam, S.; Chhabra, R. P. Can J Chem Eng 1987, 65, 1004.
27. Manjunath, M.; Tripathi, A.; Chhabra, R. P.; Sundararajan, T. Int J Engng Sci 1994, 32, 927.
28. Prasad, D.; Narayan, K. A.; Chhabra, R. P. Int J Engng Sci 1990, 28, 215.
29. Davies, C. N. Proc Inst Mech Engrs 1952, 1B, 185.
30. Han, S. T. Pulp Pap Mag Can 1969, 2, 67.
31. Ingmanson, W. L.; Andrews, B. D.; Johnson, R. C. TAPPI 1959, 42, 840.
32. Chen, C.Y. Chem Rev 1955, 55, 595.
33. Sadiq, T. A. K.; Advani, S. G.; Parnas, R. S. Int J Multiphase Flow 1995, 21, 755.
34. Dybbs, A.; Edwards, R. V. In Fundamentals of Transport Phenomena in Porous Media; Martinus Nishoff; Dordrecht, 1984; p. 199.